Spin Orientation Manipulation by Electric Fields and X-ray Irradiation

Mariia Filianina,[a,b] Weiliang Gan,[c] Tetsuya Hajiri,[d] Michael Le,[a,b] Tatiana Savchenko,[e] Sergio Valencia,[f] Mohamad-Assaad Mawass,[f] Florian Kronast,[f] Samridh Jaiswal,[a,g] Gerhard Jakob,[a] and Mathias Kläui[a,b,1]

[a] *Institute of Physics, Johannes Gutenberg University, 55128 Mainz, Germany*
[b] *Graduate School of Excellence Material Science in Mainz, 55128 Mainz, Germany*
[c] *School of Physical and Mathematical Sciences, Nanyang Technological University, 639798 Singapore*
[d] *Department of Materials Physics, Nagoya University, 464-8603 Nagoya, Japan*
[e] *Swiss Light Source, Paul Scherrer Institute, 5232 Villigen PSI, Switzerland*
[f] *Helmholtz-Zentrum Berlin für Materialien und Energie, 12489 Berlin, Germany*
[g] *Singulus Technology AG, 63796 Kahl am Main, Germany*

Received 20.04.2020, accepted 01.09.2020, published 31.10.2020

Electric field-induced strain engineering of the magnetic anisotropy offers a highly attractive perspective for designing future generations of energy-efficient information technologies. In this work, we show using x-ray magnetic imaging and magneto-optic Kerr effect that the applicability of this approach is limited to systems with comparably low magnetic anisotropies or sufficiently large magnetostrictive effect. Furthermore, we find that long x-ray exposure leads to an irreversible change of the magnetic anisotropy in thin ferromagnetic CoFeB films so caution needs to be exercised when analyzing anisotropies. While this change of the anisotropy is shown to be beneficial for the strain-induced manipulation of the magnetic structure, the mechanisms underlying the observed x-ray induced transformation remain an open question. Finally, by directly imaging the magnetic domain structure with gradually varying anisotropy from out-of-plane to in-plane, we observe the impact of strain across the spin-reorientation transition.

1 Introduction

Energy-efficient control of the magnetization state at the nanoscale is fundamental for the future generation of spintronic devices. Conventionally, the magnetization direction of ferromagnetic (FM) elements can be manipulated by electrical currents, required to generate large magnetic fields or spin torques switching the magnetization direction.[1–4] These approaches, however, suffer from significant energy dissipation due to Joule heating. Recently, the use of electric fields to manipulate the magnetic properties has emerged as a promising alternative as it avoids the need for electrical currents.[5]

Although the direct effect of electric fields, e.g. by charge doping, on the magnetic state is often relatively weak,[6] this approach can be mediated by mechanical strain, as it is commonly realized in piezoelectric/FM heterostructures.[7–9] In such systems, an electric field applied across the piezoelectric generates strain, which in turn is transferred onto an adjacent FM. The elastic deformations of the lattice in the FM layer result in the change of its magnetic anisotropy, which is known as the magnetoelastic (ME) effect, due to the ME coupling.[10] The resulting changes of the magnetic anisotropy of the material due to the strain-induced ME anisotropy can be formally expressed as follows:[11]

$$K_{\mathrm{ME}} = -\frac{3}{2}\lambda_s Y \epsilon, \tag{1}$$

where K_{ME} (J m^{-3}) is the ME anisotropy coefficient, λ_s and Y are the magnetostriction constant and the Young's modulus of the material, respectively, and ϵ is the induced strain.

It is known that the strain-induced ME anisotropy in the order of $10-100$ kJ m^{-3} can be achieved for moderate strain magnitudes of $0.1-1\%$[7,12] for some magnetostrictive materials, such as Ni, CoFeB, Ga_xFe_{1-x} films.[11] Thus, for the systems, where other anisotropy contributions are small, the strain effect can be sufficient to modify their magnetic state: for example, to switch the magnetization between an in-plane (IP) and out-of-plane (OOP) orientation under isotropic biaxial strain,[13,14] or rotate within the film plane under uniaxial in-plane strain.[15]

Moreover, the strain-induced changes of magnetic anisotropy result in changes of magnetic structures such

[1] e-mail: klaeui@uni-mainz.de

as spin structures of domain walls,[16] vortices,[7,17] and skyrmions.[18] The dynamic strain can not only drive the magnetic vortex and domain motion,[19] but also modify the mobility of a domain wall driven by conventional magnetic fields and electrical currents.[12,20] Thus, the electric field-induced strain control of magnetic anisotropy is a pathway towards low power tailoring of the magnetic properties of FM thin films and has potential advantages for future generation of magnetic devices.

However, as the strain-induced anisotropy is limited by the magnitude of the generated strain, its impact on the magnetization in the systems with large intrinsic magnetic anisotropies can be insignificant, which, in turn, hinders its observation.

In this work, we first study the effect of piezoelectric strain on the magnetic properties of a W/CoFeB/MgO thin film with a perpendicular magnetic anisotropy (PMA) deposited on a piezoelectric substrate, in the text referred to as "PMA sample" (see Methods for the details on the sample composition). We analyze the magnetization switching behavior by means of magneto-optical Kerr effect (MOKE) and perform direct imaging of the magnetic domain structure as affected by the piezoelectric strain with photoemission electron microscopy combined with x-ray magnetic circular dichroism (XMCD-PEEM). We observe that while the magnetic domain structure of the PMA sample changes locally with a non-deterministic magnetic switching, the macroscopic perpendicular magnetic hysteresis loop of the film, measured with MOKE does not show a large dependence on the applied strain.

We report that during the experiments studying the local spin structure changes using x-ray-based microscopy, an additional mechanism for change of the domain structure was observed: x-ray irradiation induces an irreversible change of the magnetic anisotropy. By comparing the observations on the PMA sample with another PMA system MgO/CoFeB/Ta, grown on a similar piezoelectric substrate (see Methods), initially exhibiting different magnetic properties but demonstrating the same behavior under irradiation, we propose possible mechanisms of the x-ray induced anisotropy change.

Finally, making use of the x-ray induced anisotropy changes we demonstrate the electric field induced strain control of the magnetic domain structure across the region of varying magnetic anisotropy in the samples close to the spin reorientation transition (SRT).

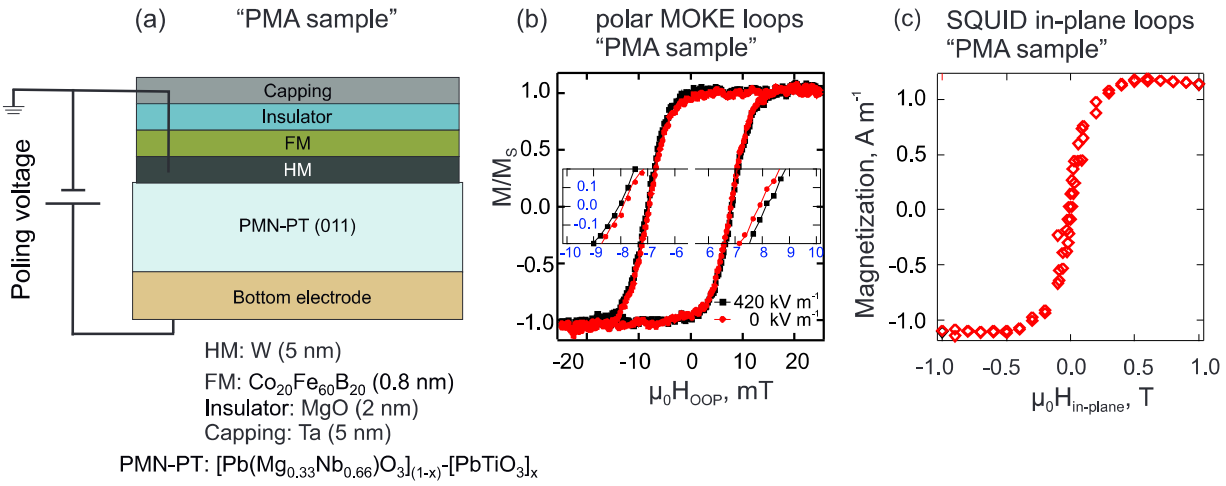

Figure 1: Schematics of the structure of (a) PMN-PT(011)/W(5)/$Co_{20}Fe_{60}B_{20}$(0.8)/MgO(2)/Ta(3) ("PMA sample"). Thickness in parentheses is given in nm. (b) Polar-MOKE hysteresis loops of the PMA sample measured at 0 kV m^{-1} (black) and 440 kV m^{-1}. The MOKE signal was collected from the area defined by the laser beam spot size when focused on the sample surface in a dot of ca. 300 μm in diameter. Note, that the PMN-PT substrate was poled before the measurements, ensuring the linear response of the generated strain to the applied electric field. The inset shows zoomed-in regions of the loops in the vicinity of the coercive fields. (c) In-plane hysteresis loop measured by SQUID for the PMA sample at 0 kV m^{-1}.

2 Electric field induced strain manipulation of the magnetization in PMA sample

To generate the mechanical strain a commercial piezoelectric substrate $[Pb(Mg_{0.33}Nb_{0.66}O_3)]_{0.68}$-$[PbTi_3]_{0.32}$ (PMN-PT) was used.[21] Uniaxial in-plane strain was generated by application of an OOP DC electric field across the piezoelectric PMN-PT(011) substrate. When an electric field is applied along the $[011]$ direction, the compressive and tensile strain along the in-plane $[100]$ and $[01\bar{1}]$ crystallographic directions of the PMN-PT substrate, respectively, are generated.[22,23]

The strain response of PMN-PT (011) to the applied electric field generally exhibits a hysteretic behavior with a large strain jump in the vicinity of the electric coercive field of the crystal (ca. 200 kV m^{-1}).[22] However, a linear regime

with smaller but electrically controllable piezoelectric strain can be used.[7,17] To promote the linear regime the substrate is poled in one direction, by an electric field larger than the coercive field (> 200 kV m^{-1}), and the linear response remains until the substrate is poled in the opposite direction, i.e. as long as the electric field does not exceed the reverse coercive field (< -200 kV m^{-1}).[22] Therefore, prior to the experiments the PMN-PT substrate was electrically poled by applying 400 kV m^{-1} and the measurements were performed using the electric field in the range from -100 kV m^{-1} to 420 kV m^{-1}. From the literature[22,23] it is known that in the linear regime, the piezoelectric coefficients along the $[100]$ and the $[01\bar{1}]$ directions of the PMN-PT substrate are approximately -890 pC N^{-1} and 290 pC N^{-1}, respectively. Furthermore, a finite OOP tensile strain, i.e. along the $[011]$ direction, can be expected based on the volume conservation,[22] which is consistent with the direct measurements by a strain gauge.[23]

The schematic structure of the PMA sample consisting of continuous film of W/$Co_{20}Fe_{60}B_{20}$/MgO/Ta on a PMN-PT (011) substrate (see Methods) is depicted in Fig. 1 (a). Black markers in Fig. 1 (b) show an OOP magnetic hysteresis loop for the PMA sample measured by polar-MOKE. The analyzed area for the MOKE measurements was approximately 300 μm, set by the laser beam spot focused on the sample surface. The hysteresis loop in red was measured under the electric field of 400 kV m^{-1} applied to the PMN-PT (011) substrate. One can see that the shape of the macroscopic hysteresis loop does not qualitatively change upon the application of strain. A slight increase of the coercive field by ca. 0.3 mT, i.e. only 3 % change, upon increasing the electric field can be observed as shown in the inset in Fig. 1 (b). This observation is consistent with the generation of small tensile strain in the OOP direction by application of an electric field as discussed above, which makes the OOP direction more energetically favorable for the magnetization of the CoFeB film with a positive magnetostriction coefficient according to Eq. 1.[25]

The anisotropy constant $K_{\text{eff}} = 0.277$ MJ m^{-3} of the PMA sample was estimated as $K_{\text{eff}} = \frac{\mu_0 H_{\text{k}} M_{\text{s}}}{2}$, where the anisotropy field $\mu_0 H_{\text{k}} = 0.5$ T and the saturation magnetization $M_{\text{s}} = 1.11 \cdot 10^6$ A m^{-1} were extracted from the IP magnetic field sweep shown in Fig. 1 (c) measured by a superconducting quantum interference device (SQUID). It is typical, that for the system with intrinsically large magnetic anisotropies, such as perpendicularly magnetized thin films, the strain needs to be of a much higher magnitude to induce a sizeable relative change in the anisotropy. Typically, strains of a few percent are required, which can only be achieved for example by mechanically bending the substrates.[24]

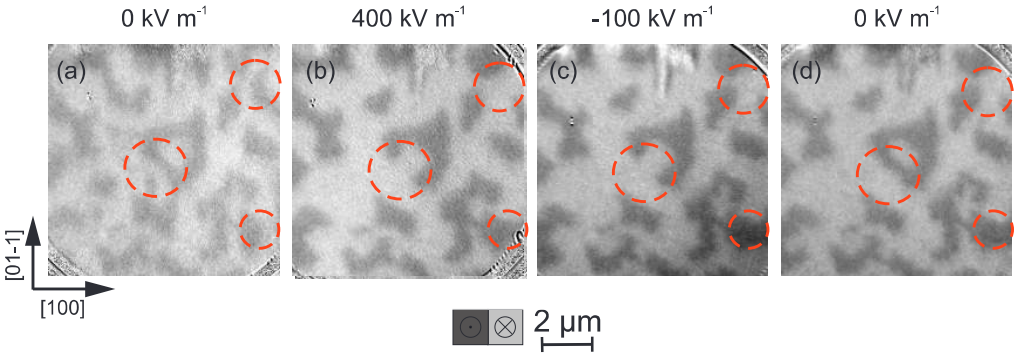

Figure 2: XMCD-PEEM images of the magnetic domain structure of the PMA sample measured at different magnitudes of the applied electric field within the linear regime of the strain response. All images were acquired at zero applied magnetic field. The red circles highlight some areas of the domain structure that switch upon changing the electric field.

However, this does not exclude that local changes of the magnetization can be generated, as previously demonstrated.[26] Figure 2 shows a series of XMCD-PEEM images of the magnetic domain structure of the CoFeB film under an applied electric field of different magnitude and at zero magnetic field. The sample was demagnetized *ex situ* prior to imaging, which led to formation of the OOP stripe domains pattern.

One can see that upon poling the domain structure remains largely unchanged, with only a small fraction of the magnetic domains switching highlighted by red circles in Fig. 2. It is clear by comparing the images in Figs. 2 (a) and (b) that the switching from *up* to *down* as well as from *down* to *up* domains occurs when the electric field is increased from 0 kV m^{-1} to 400 kV m^{-1}. In Fig. 2 (d) we can also see that some parts of the domain structure switch reversibly, but the overall domain structure does not reverse to what it was before poling in Fig. 2 (a).

We also note that the application of an electric field induced-strain does not lead to a reorientation of the magnetization from OOP to IP or *vice versa*, which would result in an additional black/white contrast level in the XMCD-

[2]Similar behavior was observed for a few other points on this sample as well as for other PMA films on PMN-PT substrates, e.g. PMN-PT(011)/W/CoFeB(0.7)/MgO/Ta, PMN-PT(011)/Pt/Co/Pt, PMN-PT(011)/Pt/Ta/Pt/MgO/CoFeB(1.1)/Ta.

PEEM images. Thus, the direct imaging results[2] suggest that most of the observed local changes are random and possibly occur due to strain-induced modification of the energy landscape. On the other hand, a small change in the coercive field seen in MOKE agrees with the observation of some local and reversible changes of the magnetic domain structure.[26]

3 X-ray induced anisotropy change

X-ray induced anisotropy change of the PMA sample As mentioned earlier, the electric field induced strain has a negligible effect on the macroscopic magnetization of the PMA film. However, after several hours of XMCD-PEEM imaging of the PMA sample, we observed that the domain structure started to change, and eventually the OOP domains transformed into a completely different domain structure with a different contrast level. Figure 3 (a) shows a zoomed-out XMCD-PEEM image acquired using a larger field of view (FOV) after this transition. The yellow dashed line indicates the approximate edge of the area exposed by the x-rays during the previous measurement in the FOV 10 μm, for which a high spatial resolution was required (e.g. those shown in Fig. 2). For that the x-ray beam size was reduced by the exit slit of the beamline, so that the footprint of the beam on the sample surface was approximately 10×20 μm set by the instrument.[27]

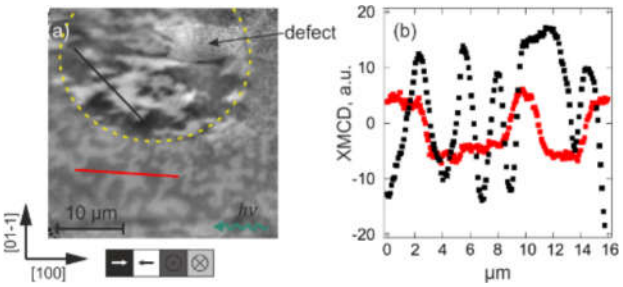

Figure 3: (a) XMCD-PEEM image using FOV of 50 μm after several hours of imaging in FOV of 10 μm showing the domains structure at 0 kV m^{-1} applied across the PMN-PT substrate and at zero applied magnetic field. (b) XMCD signal profiles along the black and red lines, showing that IP and OOP domains yield XMCD contrast of different magnitudes. The crystallographic directions of the PMN-PT substrate setting the tensile ($[01\bar{1}]$) and compressive ($[100]$) strain directions are indicated.

Thus, the area within the yellow line was exposed by the x-ray beam, and the outer area of the sample was not exposed. We see, that the unexposed region exhibits the same stripe domain structure, while the domain structure of the exposed area is dramatically different. Therefore, we can conclude that the observed local change of the domain structure was caused by the long (ca. 10 hours) exposure by the x-ray beam.

Moreover, the switched area has a noticeably different XMCD contrast level (with a much brighter/darker white/black domains) as compared to that of the OOP stripe domains. This indicates that the domains within the exposed area are more in-plane magnetized, because the low angle of incidence of the x-ray beam leads to a stronger contrast for the IP orientated magnetization. Unfortunately, the additional images corresponding to the different azimuthal angles necessary to extract the angular dependence of the XMCD contrast for these domains could not be acquired, thus we cannot conclude about the exact magnetization direction, which could be tilted between OOP and IP.

On the other hand there is a good agreement with the conclusion that the exposed area has IP magnetized domains from the quantitative comparison of the two XMCD contrast levels measured on the exposed and unexposed regions [see Fig. 3 (b)]. Because the angle of incidence of the x-ray beam is 16° from the surface plane the XMCD signal from the OOP domains should be a factor of $\tan 16^\circ \approx 0.29$ smaller than that from the IP domains, when having the same amount of the spin moment to contribute.[28] We calculate the average maximum XMCD values for the black and red profiles in Fig. 3 (b) and obtain the $\frac{I_{\text{OOP-XMCD}}}{I_{\text{IP-XMCD}}}$ ranging from ~ 0.27 to ~ 0.38. While the former value is approximately equal to $\tan 16^\circ$, which makes the assumption, that the IP magnetization in the irradiated area is along the x-ray direction and in the non-irradiated area it is fully OOP, reasonable, the latter value suggests that the magnetization does not fully lie in-plane. Alternatively, the in-plane magnetization direction may not be strictly along the x-ray beam direction, which would also result in the larger values of $\frac{I_{\text{OOP-XMCD}}}{I_{\text{IP-XMCD}}}$. Nonetheless, from this analysis we can conclude that the magnetization in the irradiated area is tilted from the OOP direction and is close to the in-plane direction.

Another interesting observation is the behavior of the stripe domains close to the exposed area. As seen from Fig. 3 (a), the average stripe domain size gradually decreases approaching the exposed area, where the magnetization lies in-plane. Similar patterns are known for thin wedge systems with a gradient thickness of the FM layer. For such systems the average domain width decreases in the vicinity of a SRT which is attributed to the the variation of the magnetic anisotropy across the thickness.[29–32] As the effective magnetic anisotropy K_{eff} decreases with increasing thickness, formation of domain walls becomes more favorable, because the domain wall energy scales with the anisotropy $\sigma_{\text{DW}} \sim \sqrt{AK_{\text{eff}}}$, where A is the exchange constant, which leads to the increasing number of domains of a smaller width.[29,32]

Based on the observed domain size behavior, we can conclude that in our system spatial variation of the magnetic anisotropy takes place. However, here, the FM layer thickness is homogeneous, therefore a different mechanism needs to be considered, which clearly is induced by the x-ray irradiation.

X-ray induced anisotropy change of the inverted sample Before we go into discussion of the possible origins of the observed behavior, we check if the x-ray induced anisotropy change is limited to this stack or occurs more widely. To this end we study a different material stack, namely Pt/Ta/Pt/MgO/$Co_{20}Fe_{60}B_{20}$/Ta, deposited on the PMN-PT(011) substrate (see Methods). The schematic structure of this sample is shown in Fig. 4 (a). Note that the order of the layers is inverted as compared to that of the previously discussed PMA system, thus we term this sample in the description below as "inverted". Here we also find a similar x-ray induced anisotropy change.

MOKE and SQUID magnetometry results, presented in Figs. 4 (b) and (c), respectively, show that in the inverted sample the PMA ($K_{\text{eff}} \approx 0.1$ MJ m^{-3}) is reduced as compared to the Ta-based stacks with a conventional order of the layers[33] and the PMA sample discussed above, thus, it is already close to the SRT before the x-ray exposure.

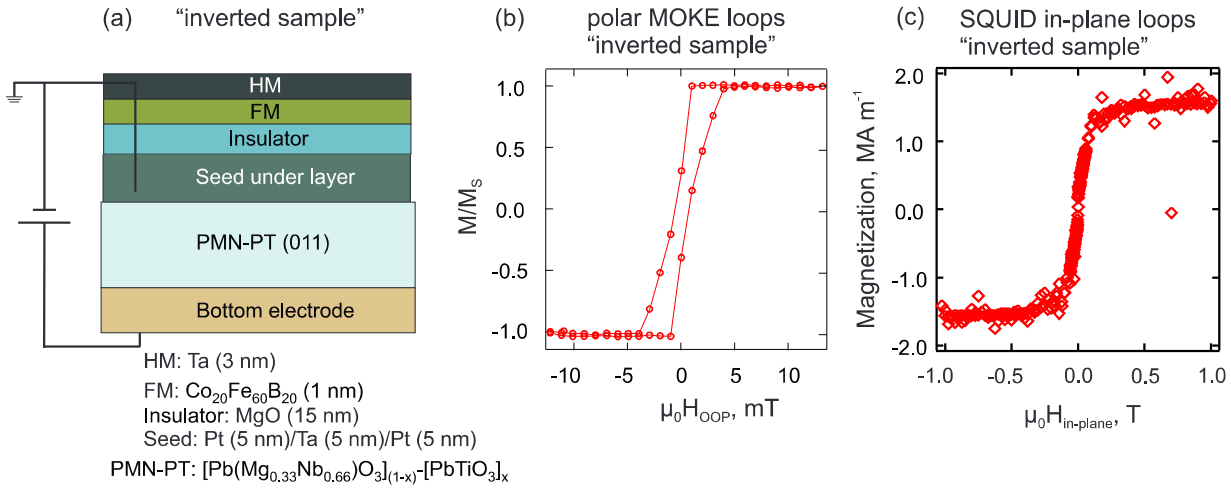

Figure 4: (a) Schematics of the structure of PMN-PT(011)/Pt(5)/Ta(5)/Pt(5)/MgO(15)/$Co_{20}Fe_{60}B_{20}$(1)/Ta(3) ("inverted sample"). Thickness in parentheses is given in nm. (b) Polar-MOKE hysteresis loops of the inverted sample measured at 0 kV m^{-1}. The MOKE signal was collected from ca. 300 μm of the sample surface, that is the laser beam spot size when focused on the sample surface. (c) In-plane hysteresis loop measured by SQUID for the inverted sample at 0 kV m^{-1}.

Prior to XMCD-PEEM imaging the inverted sample was demagnetized *ex situ* and the magnetic field was set to zero during the measurements. The domain structure of the inverted sample is shown in Fig. 5 (a), and resembles a regular stripe domain structure with an average domain size of 300 − 400 nm. With the x-ray exposure, the domain pattern disappears following the noticeable reduction of the stripe domain width. This suggests that the domains become smaller than the accessible resolution of the instrument (ca. 60 nm in XMCD mode using 10 μm FOV).

The stripe domains disappear completely after ca. 20 s of the x-ray exposure, and after ca. 200 s the new domain structure, exhibiting a stronger XMCD contrast, starts to propagate from one edge of the FOV [Fig. 5 (b)]. Note that the x-ray beam was intentionally put off the center of the FOV, thus, leading to a photon flux gradient. Switching off the x-rays for some time did not lead to recovery of the initial stripe domain phase, suggesting the same irreversible character of the x-ray induced changes of the magnetic properties, as discussed above for the PMA sample studied first.

In Fig. 5 (b) it is also possible to see that the new domains start propagating from one side of the image, i.e. from the maximum of the x-ray beam intensity. This suggests that the x-ray flux indeed governs the process. The switching occurs more readily at higher intensity of x-rays and then propagates to the edges of the beam, where the flux drops strongly.

We also note, that in this case the resulting domain structure formed with the time of the x-ray exposure clearly resembles the ferroelectric domain structure of the PMN-PT substrate known from the literature.[22] Also, similarly to the PMA system, the XMCD contrast of the stripe domains [Fig. 5 (a)] is a factor of 3 smaller than that after the irradiation-induced switching [Fig. 5 (c)], which suggests that the newly formed domains are more in-plane magnetized. Moreover, the new domains here appear only bright or dark, with no noticeable contribution of gray domains (with the magnetization perpendicular to the x-rays propagation direction). Thus, the switched area exhibits an easy axis along the x-ray direction or along one of the crystallographic axes of the cubic PMN-PT substrate.

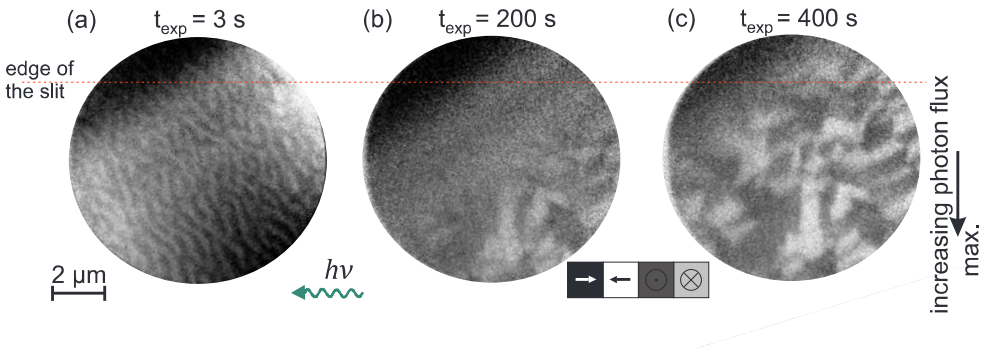

Figure 5: Snapshots of XMCD-PEEM imaging of domain structure of the inverted sample, acquired after different x-ray exposure times t_{exp} at 0 kV m^{-1} applied across the PMN-PT substrate and at zero applied magnetic field. Note that the black/white contrast in (a) is enhanced on purpose for better visibility of the domains.

4 Possible origins of x-ray induced anisotropy modification

It is known, that x-ray irradiation can alter the charge and orbital states of strongly correlated systems [34–36] and perturb the bonds of soft materials. [37] However, the materials studied here are expected to be neither of these. On the other hand, it is also known from the literature that high-energy x-rays and secondary electrons generated due to the photoeffect have a strong effect on insulating materials, [38] which compose a significant part of the systems discussed in this work (PMN-PT substrates and MgO layers are insulating). The processes which are expected to be responsible for the x-ray induced damage, can be classified as follows: (*i*) the ones which occur during the transport of the exited electrons in the material and (*ii*) those, due to the electrons emission into the vacuum.

For the former, it was shown that the core electrons/holes excited by x-rays can scatter with ions in the insulating oxide-containing layer, which leads to breaking the bonds and subsequent creation of structural defects, especially oxygen vacancies. [39] The latter leads to local charging of the irradiated area, because many electrons are emitted into vacuum. While in conductive materials, the lack of electrons is compensated within a few picoseconds, [40] in the case of insulating materials the recombination rate is strongly suppressed. Thus, the resulting uncompensated electric field can drive the migration of the mobile ions in the sample. [38,41] Moreover, the ion desorption cannot be neglected when the electric field strength is large and the electrons coming from the surroundings cannot compensate for the emission of the electrons in order to reach a stable electrostatic equilibrium. [41] On top of this, according to previous studies, also the local heating due to the deposited energy by x-rays leads to an enhanced drift and diffusion of oxygen within the system. [42] The diffusion of interstitial ions was shown in the literature to take place even at room temperature, which can lead to their aggregation into clusters, which become more stable with the size of the clusters, resulting in long-lived local structural deformations. [43]

The aforementioned processes could be relevant for our systems because the magnetic anisotropy in these stacks, originating from both interfaces of the magnetic CoFeB layer, is determined by the surrounding of the magnetic atoms. The origin of the interfacial PMA in the FM/MgO interface is partially attributed to the interfacial symmetry breaking and the hybridization between Fe(Co) $3d$ and O $2p$ orbitals. [44,45] On the other hand, the contribution from the heavy metal to the PMA is due to hybridization of both d and p orbitals at the interface via spin-orbit coupling. [46,47]

From these arguments it becomes clear that any structural modification of the interface will affect the interface-induced magnetic anisotropy. For example, it was shown that the PMA in Co/Pt systems can be altered by irradiation of the samples with He^+ or Ga^+ ions with the energies of several tens keV. [48–50] The observed behavior was attributed to the irradiation-induced short-range displacement of recoil atoms and their relaxation to new positions with local surroundings differing from their initial one, [49] which in the case of interfacial atoms, resulted in a change of the PMA in Co/Pt systems. Furthermore, ion irradiation was also shown to cause intermixing between Co and Pt in such systems, which, in turn, can result in an in-plane lattice expansion and the anisotropy change via the ME effect. [49] While on our experiment no ion irradiation was employed, x-ray irradiation-induced processes leading to local structural deformations of the MgO layer and its interface with CoFeB, could still take place, as discussed above. Therefore, we can apply similar arguments to explain the change of the magnetic anisotropy in our system.

Alternatively, recent studies report voltage control magnetic anisotropy (VCMA), which is realized when a voltage is applied across an thin oxide/FM interface. [51] This leads to a charge redistribution between the OOP and IP orbital of the FM, resulting in the change of the surface magnetic anisotropy. [45]

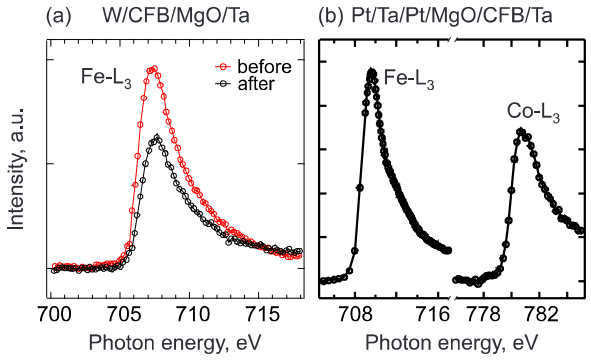

Figure 6: (a) X-ray absorption spectra (XAS) corresponding to the Fe L_3 absorption edge measured on the damaged area for the PMA sample before and after the x-ray induced SRT. (b) XAS for Fe and Co measured for the inverted sample after the exposure that leads to the reorientation of the magnetization in to the plane.

Thus, taking these facts into account we can expect that any structural or electronic change in the vicinity of the two CoFeB interfaces due to the x-ray exposure can alter the magnetic anisotropy of the system, which results in a change of the domain structure. Now we can go through the arguments, that allow us to rule out certain scenarios seemingly responsible for the observed behavior of our systems.

(*i*) Based on the shapes of the Fe and Co absorption peaks shown in Fig. 6, which were measured on the exposed area after its OOP-IP transition, we can exclude significant oxygen implantation into the CoFeB layer. In the case of Fe or Co oxidation a typical oxide shoulder feature would appear in the corresponding peaks. However, the spectra in Fig. 6 (a) do not indicate any formation of an iron oxide peak in the PMA system. Only a slight change in the intensity is observed, which can be attributed to the carbon deposition due to x-ray induced contamination.[52] Presented in Fig. 6 (b) Fe and Co absorption edges of the inverted system, corresponding to the switched area,[3] also do not exhibit oxide features.

(*ii*) As a result of the irradiation-induced ion migration, oxygen ions could also leave the MgO layer and diffuse into the adjacent non-magnetic metallic layer (for example, Ta for the PMA sample).[4] It is important to point out that a nominally similar stack as that used for the inverted sample, grown on a conductive Si substrate with only a thin natural SiO_2 layer, did not show any x-ray induced damage/change within a few days of exposure with similar photon flux. This suggests that an insulating PMN-PT substrate which also has plenty of oxygen indeed plays a role in the irradiation damage. On the other hand, this scenario could explain the local change of the anisotropy in the PMA sample.

(*iii*) It is important to keep in mind that during PEEM imaging, the sample surface is always electrically grounded [Fig. 1 (a) and (b)]. To ensure a good electrical contact the multilayer stack, containing a thick insulating MgO layer, was scratched at the sides and a drop of conducting silver paste is used to attach the sample to the sample holder body (local ground of the microscope). Therefore, all of the metallic layers on top of PMN-PT are expected to be on the same (ground) potential. Thus, the excess of positive charge due to emission of secondary electrons, can potentially be easily compensated by the conduction electrons from the metallic layers.

Below we summarize the observations discussed above, which, however, did not bring us to a conclusive understanding of the mechanisms underlying the x-ray induced OOP to IP SRT:

- The x-ray induced anisotropy modulation starts from the area with a higher photon flux;
- The anisotropy change occurs on different time scales for the PMA sample (with higher PMA, ca. 10^4 s) and for the inverted sample (with canted magnetization, ca. 200 s) for a comparable photon flux;
- Induced IP domains have a magnetic easy axis along x-rays or crystallographic directions of the PMN-PT substrate. Note that circularly polarized light was used, i.e. no defined electric field direction could be imposed on the domain structure;
- A gradual change of the domain structure is observed indicating a gradual change of the anisotropy;
- The sample surface is always electrically grounded providing a source of electrons to prevent charging;
- Fe, Co peaks do not have features typical for oxides within the resolution;
- Demagnetization of the samples by cycling an external magnetic field does not help to recover the stripe domain phase, signifying a permanent structural character of the x-ray induced changes;
- For inverted stack grown on Si/SiO_2 substrate the x-ray induced SRT does not occur within (at least) 3 days of exposure.

Despite the argument that the sample surface is always grounded, the most plausible mechanism of the x-ray induced SRT in our system relies on local charging due to the lack of the electrons and inability of thin conductive layer as compared to an insulating bulk to compensate for this. This charging, leading either to the displacement of ions as well as local charge redistribution on the orbitals at the CoFeB interface which determine the magnetic anisotropy of the systems, results in the decrease of the PMA and the associated OOP to IP transition.

[3]The SRT occurs much faster (ca. 20 s) than the time necessary to acquire one XAS (ca. 5 min).
[4]The absorption peak of Mg after the SRT was not measured.

5 Strain induced changes of the domain structure close to the SRT

In this section, we consider again the PMA sample, where we can take advantage of the modified magnetic anisotropy by the x-ray exposure to be sensitive to small strain-induced anisotropy change. The irradiated areas allow us to simultaneously investigate the impact of strain on the domain structure at the regions with different magnetic anisotropies, from IP to OOP. As discussed above, the electric field induced strain does not influence the OOP domain structure. However, as in the region close to the SRT, the magnetization is canted from the OOP direction, a larger effect of strain on the domain structure can be expected. It is important to note that while the absolute strain-induced anisotropy change is the same, close to the SRT, where the anisotropy is suppressed, the relative effect on the magnetization alignment is larger.

Figure 7 shows a series of XMCD-PEEM images of the area close to the SRT, including the OOP and IP magnetized regions. We can see that the entire IP region changes contrast from black/white to gray, while the OOP region remains the same. The observed change is mostly reversible and volatile, i.e. when the electric field is removed, the domain structure changes again, but with a new distribution of the domains. While the individual domains do not switch to the original state after removing the electric field, the magnetic anisotropy favoring black and white IP domain recovers.

We also note that the border between the IP and the OOP magnetized regions at 0 kV m^{-1} shifts by a few μm after the first electric field cycle (0-400-0 kV m^{-1}). But it stays nearly at the same place after the second field cycle (0-500-0 kV m^{-1}). However, it is not straightforward to conclude whether this is induced by strain or by the x-ray exposure.

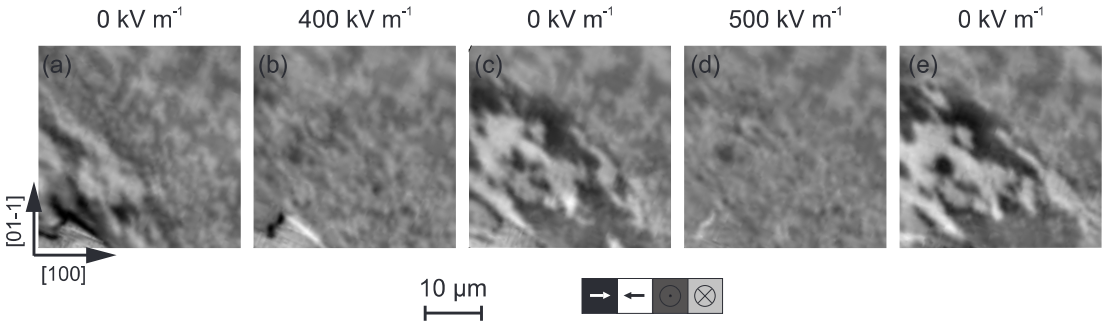

Figure 7: Set of XMCD-PEEM figures of the domain structure of the PMA sample, where part of the FOV underwent a SRT due to the x-ray exposure, acquired at different magnitudes of the applied electric field across the PMN-PT substrate. All images were acquired at zero applied magnetic field. The crystallographic directions of the PMN-PT substrate setting the tensile ($[01\bar{1}]$) and compressive ($[100]$) strain directions are indicated.

To analyze in more detail the character of the strain induced switching observed in the IP region, we quantitatively consider the change of the XMCD contrast of the individual domains in the images in Fig. 7. The results are summarized in Fig. 8 (a), where the XMCD contrast as a function of the cycling electric field is plotted for several areas. All analyzed areas are indicated in Fig. 8 (b) and Fig. 8 (c) shows zoomed-in regions of the considered domains. The value of the XMCD contrast was calculated as the average over a selected area corresponding to one domain at all values of the electric field.[5]

Here we can see that at least five distinct states can be differentiated from the contrast, which are shown shaded in Fig. 8 (a), i.e. IP-white, IP-black, OOP-bright, OOP-dark and IP-gray. The latter corresponds to the domains with the magnetization perpendicular to the x-ray direction, which yields zero XMCD contrast.

In Fig. 8 we can observe random switching of the IP domains to OOP (corresponding to IP-white to OOP-bright switching events) or 90° rotation of the IP domains (corresponding to IP-white to IP-gray switching events) in the regions in the vicinity of the domain walls. On the other hand, it can be seen that the magnetization in the middle of a domain at 0 kV m^{-1} (e.g. region "3"), is likely to remain not switched upon application of strain. This may be an indication of the inhomogeneities within the irradiated area, i.e. local pinning sites or the induced strain inhomogeneities,[8] leading to locally varying magnetic anisotropy. Thus, for some domains the generated ME anisotropy is enough to alter the magnetization state, while it is not for the others. For comparison, we also plot the XMCD contrast evaluated for non-irradiated areas "6" and "7", which do not show any variation with the electric field strength and provide a reference for the OOP-bright and OOP-dark levels indicated in Fig. 8 (a).

Moreover, the global behavior of the domain structure within the irradiated area, i.e. where the PMA is strongly suppressed, is consistent with that governed by the ME effect. As the initial state at zero strain (i.e. 0 kV m^{-1}) is mostly IP magnetized, the generation of strain (compressive along the $[100]$ and tensile along the $[01\bar{1}]$ and $[011]$ directions) upon increasing the electric field leads to cant-

[5] Within these areas the mean deviations were not larger than 10%, thus ensuring the pixels belong to the same domain at each electric field value.

ing of the magnetization of the CoFeB layer with a positive magnetostriction coefficient to the OOP direction (or its 90° rotation in-plane towards the tensile direction). Thus, the domain structure at 400 kV m^{-1} and 550 kV m^{-1} [Figs. 7 (b) and (d)] looks mostly gray with either small OOP domains or IP domains with the magnetization perpendicular to the x-ray direction.

We also note that unfortunately due to small size of the irradiated area demonstrating the SRT, we could not find the same spot in MOKE to study directly the impact of the strain on the magnetic anisotropy by corresponding magnetometry measurements.

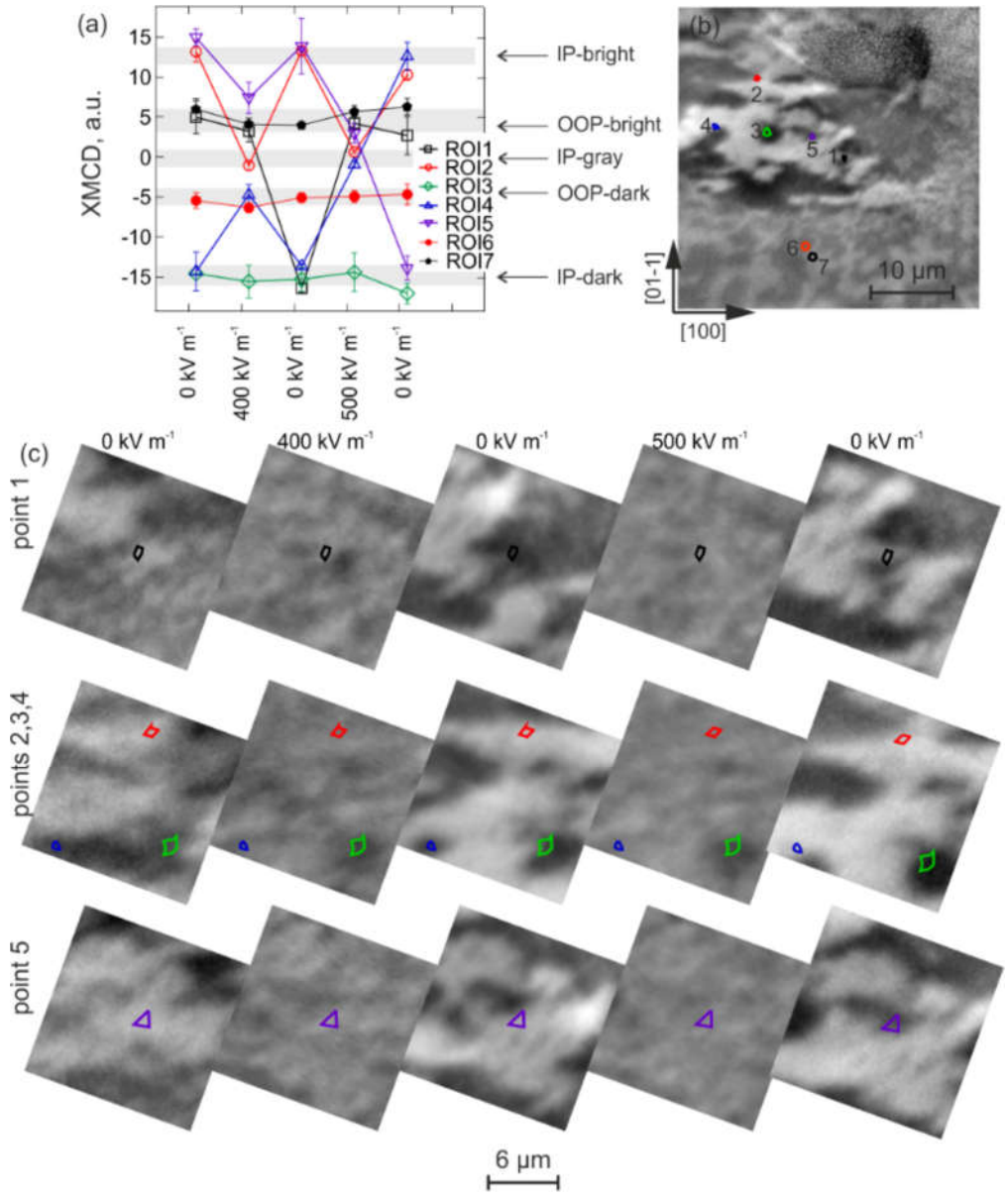

Figure 8: (a) XMCD contrast of the selected regions entailed by the magnetic domains of the PMA sample, showing the strain induced switching between five possible magnetization directions. (b) The same as in Fig. 7 (e) XMCD-PEEM image showing all analyzed in (a) regions. (c) The same as in Fig. 7 zoomed-in XMCD-PEEM images showing in detail the analyzed in (a) regions.

6 Conclusions

In conclusion, while the small impact of strain on the macroscopic perpendicular magnetic state of the PMA sample measured by the hysteresis loop did not come as a surprise, the x-ray induced modulation of the magnetic anisotropy observed for both the PMA sample and the inverted sample, is unexpected. As a result of this irreversible effect of the x-ray exposure, the domain structure of the irradiated region of the PMA sample indicates that the effective magnetic anisotropy of the system is gradually changing from an easy perpendicular axis to an easy in-plane

anisotropytowards the region exposed with the highest photon flux. On the contrary, the magnetic anisotropy of the unexposed area did not change. The attempt to explain this spatially inhomogeneous magnetic anisotropy variation, which clearly was induced by the x-ray irradiation, did not allow us to conclude on a clear mechanism. However, the resulting gradient of the magnetic anisotropy on such a small length scale allowed us to observe the effect of the strain induced ME anisotropy on the magnetic domain structure, where the strain-induced K_{ME} comparable to the effective anisotropy of the film was able to alter its magnetization state.

7 Methods

W(5)/$Co_{20}Fe_{60}B_{20}$(0.8)/MgO(2)/Ta(5) continuous films, referred to as *PMA sample*, and Pt(5)/Ta(5)/Pt(5)/MgO(15)/$Co_{20}Fe_{60}B_{20}$(1)/Ta(3), referred to as *inverted sample*, were sputter-deposited on top of a bare unpoled two-sides polished piezoelectric PMN-PT(011) substrate. Here and below the thickness in parentheses is in nm.The bottom contact of Cr(5)/Au(50) was deposited by DC sputtering in Ar atmosphere. Before the XMCD-PEEM and MOKE measurements the PMN-PT substrates with already deposited films were electrically poled by applying 400 kV m^{-1} across the substrate to promote the linear response regime of the generated strain. During the experiments the electric field was ranging from -100 kV m^{-1} to 420 kV m^{-1}, thus not exceeding the opposite electric coercive field.

Part of the experiments were carried out at SIM beamline of Swiss Light Source (SLS) as well as at UE49-PGM beamline of Helmholtz-Zentrum Berlin (Bessy). The samples were illuminated by circularly polarized x-ray beam at $16°$ angle of incidence. For XMCD-PEEM imaging the photon energy was set to 708 eV and 710 eV corresponding to the Fe L_3 absorption peak for the PMA sample and the inverted sample, respectively. The secondary electrons were detected by a commercial PEEM/LEEM setup. XMCD-PEEM images were obtained using the formula for the asymmetry $\frac{(I_+ - I_-)}{(I_+ + I_-)}$, which is proportional to $\cos\alpha$, where α is the angle between the directions of the incident circularly polarized x-rays and the film magnetization. $I_{+(-)}$ are the images acquired with circular positive (negative) polarization of the x-rays. All XMCD-PEEM images were acquired at zero magnetic field.

XMCD-PEEM imaging of the PMA sample was carried out at Bessy with a nominal x-rays beam flux at 1 keV of approximately 5×10^{13} photons/s/100mA.[53] The inverted sample was imaged at SLS with a flux of approximately 2.5×10^{14} photons/s/100mA.[54]

Prior to XMCD-PEEM imaging of the PMA sample the Ta capping layer was partially removed *in situ* by Ar^+ sputtering at the Ar pressure inside the chamber of 5×10^{-5} and the energy of 1 kV for 30 minutes. Based on the sputtering rate calibrations, ca. 2 nm of Ta were removed, which was sufficient to probe the underlying CoFeB layer without altering its magnetic properties. For the inverted sample this procedure was not necessary, as the Fe absorption edge was sufficiently intense (ca. 30%) to obtain a reasonable XMCD contrast.

Acknowledgments

The work was financially supported by the Deutsche Forschungsgemeinschaft (DFG, German Research Foundation) in particular by Grant No. KL1811/18 (318612841), the Graduate School of Excellence "Materials Science in Mainz" (DFG/GSC266) and the Swiss National Science Foundation (SNSF) (No. 200021_160186). The authors thank Helmholtz-Zentrum Berlin (HZB) and Swiss Light Source (SLS) for the allocation of synchrotron radiation beamtimes. The authors thankfully acknowledge the HZB and SLS staff for technical support. The authors would like to thank Dr. C.A.F. Vaz and Dr. A. Kleibert for fruitful discussions. The authors also achnowledge the support by the Max Planck Graduate Center with the Johannes Gutenberg Universität Mainz (MPGC) funded by the DFG (TRR173-268565370).

Bibliography

[1] Åkerman, J.; *Science*, **2005**, *308*, 508.
[2] Ralph, D. and Stiles, M.; *J. Magn. Magn. Mater.*, **2008**, *320*, 1190.
[3] Miron, I. M. et al.; *Nat. Mater.*, **2010**,*9*, 230.
[4] Boulle, O.; Malinowski, G.; Kläui, M.; *Mater. Sci. Eng.*, **2011**, *72*, 159.
[5] Wang, K. L.; Alzate, J. G.; Khalili Amiri, P.; *J. Phys. D: Appl. Phys.*, **2013**, *46* 074003.
[6] Fiebig, M.; *J. Phys. D: Appl. Phys.*, **2005**, *38*, R123.
[7] Finizio, S. et al.; *Phys. Rev. Appl.*, **2014**, *1*, 021001.
[8] Buzzi, M. et al.; *Phys. Rev. Lett.*, **2013**, 111, 027204.
[9] Lahtinen, T.; Franke, K.; van Dijken, S.; *Sci. Rep.*, **2012**, 2, 258.
[10] Kittel, C.; *Rev. Mod. Phys.*, **1949**, 21, 541.
[11] Weiler, M. et al.; *New J. Phys.*, **2009**, *11*, 013021.
[12] Shepley, P. et al.; *Sci. Rep.*, **2015**, *5*, 7921.
[13] Wang, J.; Hu, J.-M.; Chen, L.-Q.; Nan, C.-W.; *Appl. Phys. Lett.*, **2013**, *103*, 142413.
[14] Pertsev, N.; *Rep. Prog. Phys.*, **2008**, *78*, 212102.
[15] Hu, J.-M. and Nan, C. W.; *Phys. Rev. B*, **2009**, *80*, 224416.
[16] Hämäläinen, S. J. et al.; *Nat. Commun.*, **2018**, *9*, 4853.
[17] Filianina, M. et al.; *Appl. Phys. Lett.*, **2019**, *115*, 062404.
[18] Shibata, K. et al.; *Nat. Nanotechnol.*, **2015**, *10*, 306.
[19] Foerster, M. et al.; *Nat. Commun.*, **2017**, *8*, 407.
[20] Lei, N. et al.; *Nat. Commun.*, **2013**, *4*, 1378.
[21] https://www.mtixtl.com/PMNT-001-101005S1.aspx
[22] Wu, T. et al.; *J. Appl. Phys.*, **2011**, *109*, 124101.
[23] Lo Conte, R. et al; *Nano Lett.*, **2018**, *18*, 1952.
[24] Ota, S. et al.; *Appl. Phys. Express*, **2016**, *9*, 043004.
[25] Wang, D. et al.; *J. Appl. Phys.*, **2005**, *97*, 10C906.
[26] Gopman, D. et al.; *Sci. Rep.*, **2016**, *6*, 27774.

[27] https://www.helmholtz-berlin.de/forschung/oe/em/m-dynamik/forschungsgruppen/x-peem/instrumente/beamline_en.html
[28] Kuch, W. et al.; *Phys. Rev. B*, **2000**, *62*, 3824.
[29] Fukumoto, K. et al.; *Surf. Sci.*, **2002**, *514*, 151.
[30] Speckmann, M.; Oepen, H. P.; Ibach, H.; *Phys. Rev. Lett.*, **1995**, *75*, 2035.
[31] Kronseder, M. et al.; *Nat. Commun.*, *2015*, *6*, 6832.
[32] Meier, T. N. G.; Kronseder, M.; Back, C. H.; *Phys. Rev. B*, **2017**, *96*, 144408.
[33] Lo Conte, R. et al.; *Appl. Phys. Lett.*, **2014**, *105*, 122404.
[34] Poccia, N. et al.; *Nat. Mater.*, **2011**, *10*, 733.
[35] Kiryukhin, V. et al.; *Nature*, **1997**, *386*, 813.
[36] Chang, S. H. et al.; *ACS Nano*, **2014**, *8*, 1584.
[37] Analytis, J. G. et al.; *Phys. Rev. Lett.*, **2006**, *96*, 177002.
[38] Cazaux, J.; *Ultramicroscopy*, **1995**, *60*, 411.
[39] Mulroue, J. and Duffy, D. M.; *P. Roy. Soc. A: Math. Phys.*, **2011**, *467*, 2054.
[40] Krasheninnikov, A. V. and Nordlund, K.; *J. Appl. Phys.*, **2010**, 107, 7.
[41] Cazaux, J.; *J. Microsc.*, **1997**, *188*, 106.
[42] Chen, G. Z. et al.;*Nature*, **2000**, *407*, 361.
[43] Uberuaga, B. P. et al.; *Phys, Rev. B*, **2005**, *71*, 104102.
[44] Ikeda, S. et al.; *Nat. Mater.*, **2010**, *9*, 721.
[45] Wang, W. G.; Li, M.; Hageman, S.; Chien, C. L.; *Nat. Mater.*, **2012**, *11*, 64.
[46] Peng, S. et al.; *Sci. Rep.*, **2015**, *5*, 18173.
[47] Kim, S. et al.; *Appl. Phys. Express*, **2017**, *10*, 073006.
[48] Chappert, C. et al.; *Science*, **1998**, *280*, 1919.
[49] Sakamaki, M. et al.; *Phys. Rev. B*, **2012**, *86*, 024418.
[50] Sapozhnikov, M. et al.; *Materials*, **2020**, *13*, 99.
[51] Nikonov, D. E. and Young, I. A.; *J. Mater. Res.*, **2014**, *29*, 2109.
[52] Chauvet, C. et al.; *J. Synchrotron Rad.*, **2011**, *18*, 761.
[53] https://www.helmholtz-berlin.de/forschung/oe/em/m-dynamik/forschungsgruppen/x-peem/instrumente/beamline_en.html.
[54] https://www.psi.ch/en/sls/sim/beamline-layout.